

RESEARCH ARTICLE

Software for Evaluating Ionic Conductivity of Inorganic–Polymer Composite Solid Electrolytes

Yuqing Ding¹, Bing He², Da Wang¹, Maxim Avdeev^{3,4}, Yajie Li¹, and Siqi Shi^{1,5*}

¹School of Materials Science and Engineering, Shanghai University, Shanghai 200444, China. ²School of Computer Engineering and Science, Shanghai University, Shanghai 200444, China. ³Australian Nuclear Science and Technology Organisation, Sydney 2232, Australia. ⁴School of Chemistry, The University of Sydney, Sydney 2006, Australia. ⁵Materials Genome Institute, Shanghai University, Shanghai 200444, China.

*Address correspondence to: sqshi@shu.edu.cn

Inorganic–polymer composite solid electrolytes (IPCSEs) obtained by filling the polymer matrix with inorganic materials usually have higher ionic conductivity compared with individual phases. This important increase in ionic conductivity is explained in terms of the new percolation paths formed by the highly conductive interface between inorganic filler and polymer. The conduction in such systems can be investigated using the effective medium theory (EMT) and random resistance model (RRM). EMT can be used to analyze the effect of filler size on the ionic conductivity of disordered IPCSEs, while RRM can describe the composites with inorganic fillers of various shapes (nano-particles, nano-wires, nano-sheets, and nano-networks) in ordered or disordered arrangement. Herein, we present software evaluating the ionic conductivity in IPCSEs by combining EMT and RRM. The approach is illustrated by considering the size, shapes, and arrangements of inorganic fillers. The ionic conductivities of different types of IPCSEs are predicted theoretically and found in good agreement with the experimental values. The software can be used as an auxiliary tool to design composite electrolytes.

Introduction

Rechargeable lithium-ion batteries (LIBs) are widely used in daily life because of their high energy density, long cycle life, good reliability, and low cost; as a result, they find application in electronic products, electric vehicles, power grid-storage, etc. However, due to the thermodynamic instability and flammability of liquid electrolytes, safety is a serious issue for LIBs. All-solid-state rechargeable LIBs with solid electrolytes are a promising alternative for ensuring safety [1]. The generally used solid electrolytes are polymer electrolytes [2–4], inorganic electrolytes [5–9] (mainly oxide-based or sulfide-based electrolytes), and composite electrolytes [1,10]. In 2020, we made a detailed introduction and review of these solid electrolytes [1]. Here, we briefly summarize the advantages and disadvantages of these solid electrolytes (Table S1).

A solid polymer electrolyte is composed of a polymer matrix and salt, which can be approximately regarded as a solid solution system formed by directly dissolving salt in polymer. Common polymer matrices are poly(ethylene oxide) (PEO) [11], polyacrylonitrile (PAN) [12], and poly(vinylidene fluoride) [13]. Polymer electrolytes have excellent characteristics such as superior flexibility, low interfacial resistance, and low cost. Unfortunately, the low ionic conductivity of polymer

electrolytes at room temperature (10^{-7} to 10^{-5} S cm⁻¹) cannot meet the requirement of LIBs.

Oxide-based inorganic electrolytes, such as NASICON-type [14] $\text{Li}_{1+x}\text{Al}_x\text{Ti}_{2-x}(\text{PO}_4)_3$ (LATP), $\text{Li}_{1+x}\text{Al}_x\text{Ge}_{2-x}(\text{PO}_4)_3$ (LAGP), perovskite-type [15] $\text{Li}_{3x}\text{La}_{2/3-x}\text{TiO}_3$ (LLTO), and garnet-type $\text{Li}_7\text{La}_3\text{Zr}_2\text{O}_{12}$ (LLZO) [6,7,16,17], have higher ionic conductivity, excellent mechanical strength, and wide electrochemical stability window. However, these conductors are highly brittle and have a high interfacial impedance between the electrolyte and electrode [18]. The development of composite materials of inorganic and polymer electrolytes, namely, inorganic–polymer composite solid electrolytes (IPCSEs), is an effective strategy to solve the above-mentioned problems and to obtain higher ionic conductivity, ionic transference number, thermal stability, electrochemical stability, and flexibility at the same time [1].

As shown in Fig. 1, there are 3 categories of Li ions' migration paths in IPCSEs: polymer matrix phase, inorganic filler phase, and polymer/inorganic filler interface. The contribution of different migration paths and overall conductivity depend on the composition of the IPCSEs, especially the fraction of the inorganic filler. If Li ions preferentially migrate in the polymer matrix, the fillers can have an insignificant or even negative contribution to the overall ionic conductivity, so the ionic

Citation: Ding Y, He B, Wang D, Avdeev M, Li Y, Shi S. Software for Evaluating Ionic Conductivity of Inorganic–Polymer Composite Solid Electrolytes. *Energy Mater. Adv.* 2023;4:Article 0041. <https://doi.org/10.34133/energymatadv.0041>

Submitted 16 May 2023
Accepted 14 June 2023
Published 10 July 2023

Copyright © 2023 Yuqing Ding et al. Exclusive licensee Beijing Institute of Technology Press. No claim to original U.S. Government Works. Distributed under a Creative Commons Attribution License 4.0 (CC BY 4.0).

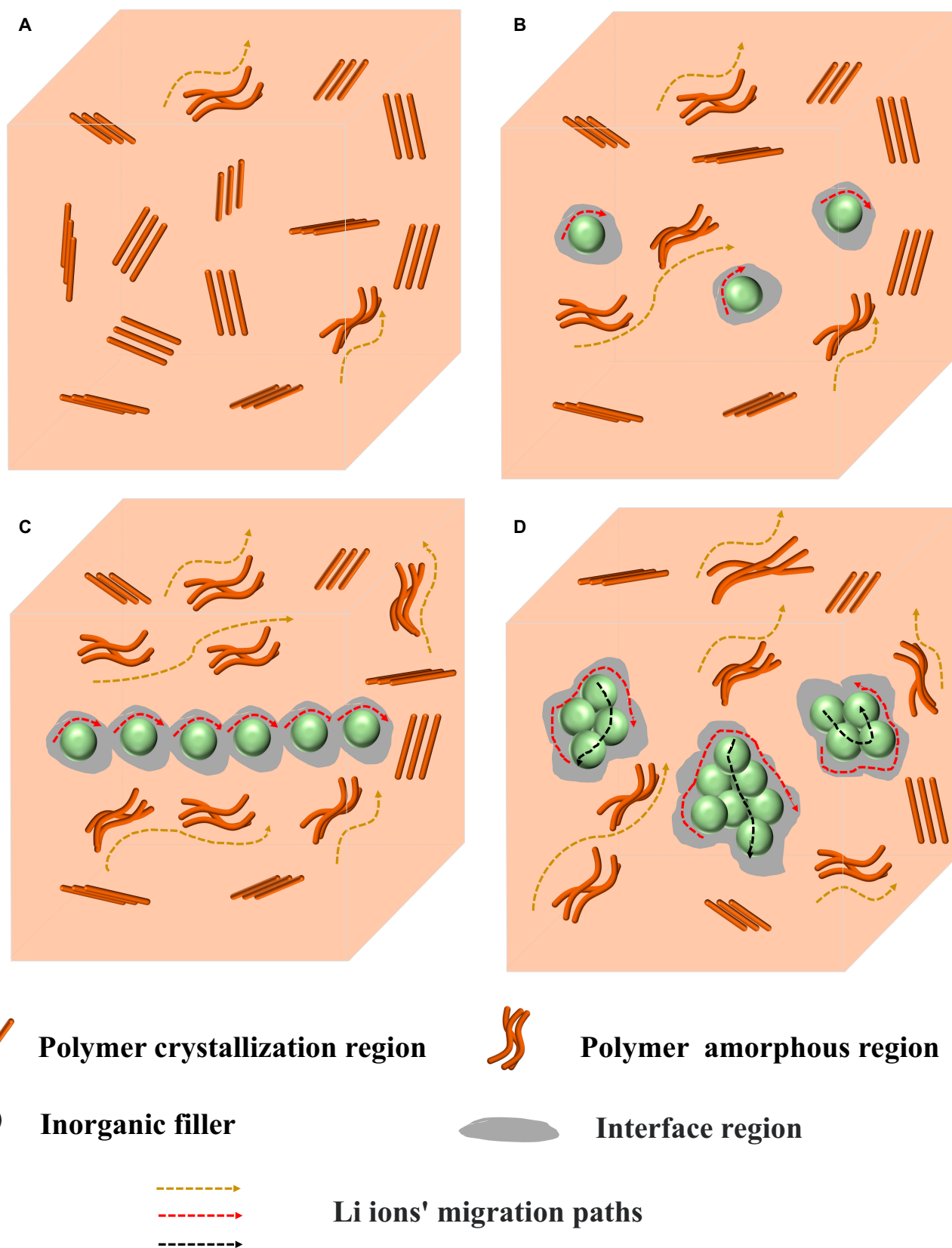


Fig. 1. Schematic diagram of the Li ions' migration path with the increased concentration of inorganic filler (the concentration of inorganic filler increased from (A) to (D)).

conductivity of the IPCSEs may be low [19,20]. In contrast, if the polymer/inorganic–filler interface is the preferential Li ions' migration path, the ionic conductivity of IPCSEs is quite high at room temperature and the filler has a positive effect on the ionic conductivity [21,22]. It should be emphasized that the systems investigated in this work are all the latter kind.

The main reason for the enhanced ionic conductivity of such IPCSEs is the formation of new highly conductive percolation paths: polymer/inorganic filler interface phase [12,23]. This significant increase in ionic conductivity can be rationalized as follows: the polymer matrix surrounding the inorganic filler tends to form amorphous regions, allowing easy lithium ion migration and facilitating ion conduction [24–26]; in addition, there is a strong Lewis acid–base interaction at the polymer/inorganic filler interface, which greatly promotes the dissociation of lithium salts. When the dissociated anions are adsorbed onto the surface of the inorganic filler, that leads to an increase in the concentration of free Li ions at the interface [24,27,28]; the acidic groups on the surface of the inorganic filler interact with the polar groups of the polymer, weakening the complexation of Li ions with the polar groups [27–29].

Given these beneficial interface effects, it follows that if the morphology of inorganic fillers is regulated to form interface paths with different shapes in IPCSEs, the ionic conductivity of IPCSEs can be enhanced. The effect of inorganic filler morphology on the ionic conductivity of IPCSEs has been confirmed by experimental studies [12,30,31]. Although experimental study is the ultimate approach, testing a large number of materials and their combinations remains a challenge and it is more convenient and efficient to evaluate the ionic conductivity of candidate composite conductors through theoretical calculations [32].

The commonly used theoretical calculations assume inorganic fillers in the form of isotropic nano-particles (NPs, Fig. 2A). Other shapes of inorganic nanofillers, such as nano-wires (NWs, Fig. 2B), nano-sheets (NSs, Fig. 2C), and nano-networks (NNs, Fig. 2D), are less often considered. Calculations can be done using the random walk method based on the random resistance model (RRM) [33–35] and the effective medium theory [32,36] (EMT). The RRM emphasizes the role of an enhanced interface conductivity and records the random walk process of walkers, which is then translated into ionic conductivity of IPCSEs via the Nernst–Einstein equation. The EMT is based on the mean field theory in which the interaction between adjacent particles is considered as a constant far field and the specific near field effect is excluded. Therefore, it is only suitable for heterogeneous systems with low inorganic filler content. Nan et al. [36–38] proposed an improved and simplified EMT to extend its applicability by including the dipole–dipole interactions between particles.

In this work, we use RRM to establish IPCSEs models of inorganic fillers with different shapes (NPs, NWs, NSs, and NNs) in the case of both ordered and disordered filling, and calculate the ionic conductivity of IPCSEs based on the De Gennes ant random walk method and the Nernst–Einstein equation. Then, we use the improved EMT [36,38] to study the effect of different sizes of inorganic fillers on the ionic conductivity of IPCSEs. In addition to calculating the ionic conductivity of IPCSEs with active inorganic fillers, we also predicted the ionic conductivity of IPCSEs with inert fillers (Al_2O_3 and SiO_2). Table S2 shows the reference experimental

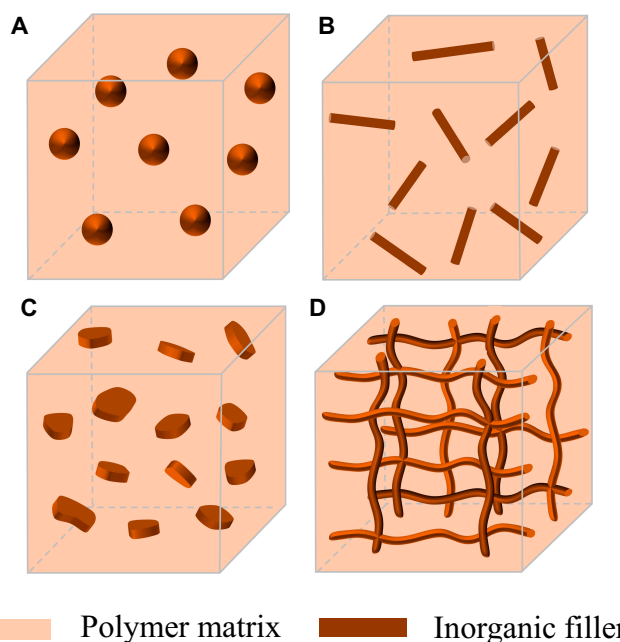


Fig. 2. Schematic diagram of composite conductors with 4 shapes of inorganic fillers: (A) nano-particles; (B) nano-wires; (C) nano-sheets; (D) nano-networks.

ionic conductivity of the component phases [including polymer matrix, inorganic filled phase, and amorphous polymer (polymer/inorganic filler interface)] at room temperature from literature.

Methods

Calculation of ionic conductivity based on random resistance model

Model building

The RRM can describe the percolation conduction in IPCSEs, and the ionic conductivity σ can be determined as a function of inorganic phase concentration p by random walk method. The RRM principle is illustrated in Fig. 3, which shows a simple cubic lattice with the size of $L \times L \times L$ divided into L^3 unit lattice sites with the size of $(1/L)^3$. The sites in the cubic lattice are randomly occupied with probability p to represent the filling of inorganic fillers (dark green cubes in Fig. 3) in IPCSEs, so the polymer sites are randomly occupied with the probability of $1 - p$ (light green cubes in Fig. 3). The 12 bonds around each lattice site (edges of each cube) are considered as resistance. There are 3 types of bonds in the cubic lattice: (a) When the 4 sites around the bond are all polymer phases, the central bond corresponds to the polymer conductivity, σ_A (A-bonds [blue] in Fig. 3A); (b) when the 4 lattice sites are all inorganic fillers, the central bond corresponds to the inorganic phase conductivity, σ_B (B-bonds [red] in Fig. 3B); (c) in all the remaining cases, the central bond corresponds to the interfacial phase conductivity, σ_C (C-bonds [black] in Fig. 3B and C). According to the fractions of inorganic fillers and polymers, the occupation probabilities of 3 types of bonds are obtained: A-bonds, $p_B^{(A)} = p^4$; B-bonds, $p_B^{(B)} = (1 - p)^4$; C-bonds, $p_B^{(C)} = 1 - p^4 - (1 - p)^4$. Therefore, RRM has 2 percolation thresholds p' and p'' . p' is the first percolation threshold, which represents the lowest concentration of inorganic

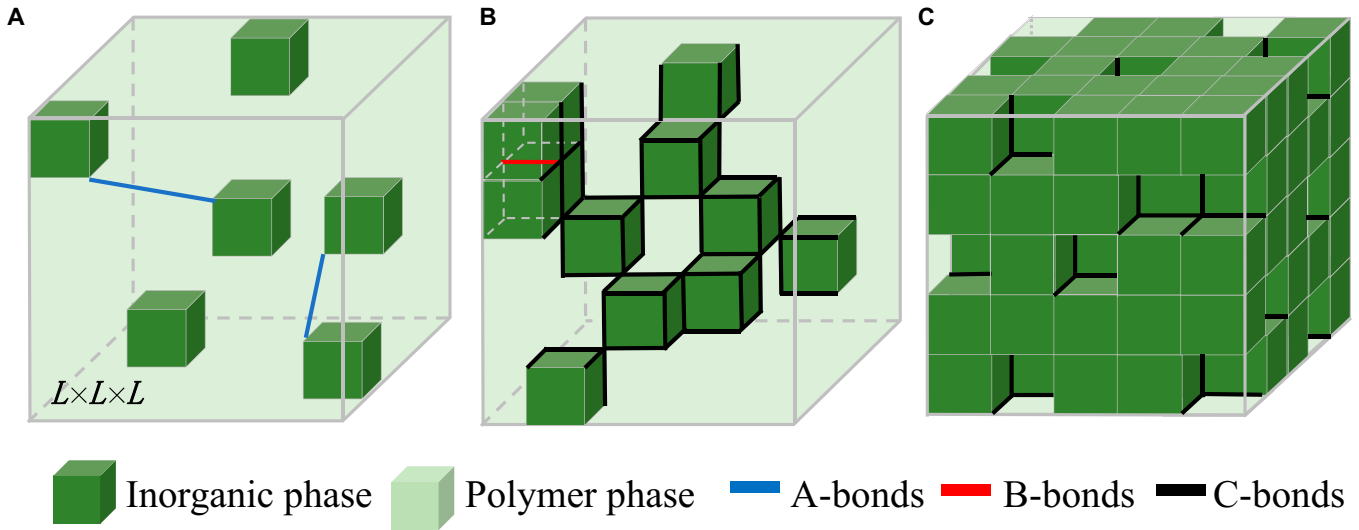


Fig. 3. Three-dimensional lattice bonds percolation diagram: (A) $p < p'$; (B) $p' \leq p < p''$; (C) $p \geq p''$. A-, B-, and C-bonds correspond to conductivities of polymer phase, inorganic filler, and interface, respectively. p represents the concentration of inorganic filler, p' is the first percolation threshold, indicating that the interface seepage conduction path begins to form, and p'' is the second percolation threshold, indicating that the interface seepage conduction path is truncated. L is the size of the lattice model.

filler phase when the highly conductive interface bonds long-range conduction network begins to form (Fig. 3B). This value is related to the concentration of high-conductivity interface bonds, so it is also called interface percolation. p'' is the second percolation threshold, corresponding to the concentration of the inorganic filler phase when all long-range high-conductivity interface bonds and long-range polymer phase bonds are disconnected (Fig. 3C). The relationship between the total ionic conductivity σ of IPCSEs and the inorganic filler concentration p can be qualitatively understood according to Fig. 3. When $p < p'$ (Fig. 3A), σ increases with the increase of highly conductive C-bonds. When $p = p'$ (Fig. 3B), the percolation path of C-bonds is formed, and σ begins to increase significantly. As p continues to increase, σ will increase to a maximum value until $p = p''$, at which level all long-range high-conductivity conduction paths are interrupted, and σ stops increasing. When $p > p''$ (Fig. 3C), the inorganic filling phase occupies most of the lattice sites of the cubic lattice, and σ decreases.

Calculation of ionic conductivity

In this work, $L = 500$, and therefore, the simple cubic lattice size is $500 \times 500 \times 500$. Evaluating the conductivity of this large-scale lattice network composed of 2-phase composites is a significant challenge. Kirchhoff's law directly analyzes circuits formed by conducting particles via construction and solution of a large number of linear systems of equations, which entails a significant time cost. A more effective method is to track and record the randomly moving walkers in the lattice, and then calculate their diffusion properties through the Nernst–Einstein equation [39,40].

The random walk method was originally proposed by De Gennes [39] to deal with the percolation effect in the composite network system. This method assumes that some microscopic “ants” are lost in the maze of nodes connected by bonds and walk randomly along these bonds [41,42]. In this work, the ionic conductivity of IPCSEs is obtained by this random walk method, assuming the “ant” to be a random walker, i.e., “blind ant” [43]. In the cubic lattice, the walkers migrate between the

endpoints of the bonds. The migration rates corresponding to the 3 types of bonds in the system are τ_A^{-1} , τ_B^{-1} , and τ_C^{-1} , and are proportional to the conductivity of the corresponding bonds (σ_A , σ_B , σ_C). Walker selects one of the 6 directions of its endpoint (front, back, left, right, up, and down) for migration. The migration rule is that walker at the endpoint has 6 migration modes, $h = 1, \dots, N_{hops}$, and the corresponding migration rate is τ_h^{-1} . Generate a random number $\zeta \in (0, 1)$, and determine migration events H according to Eq. 1:

$$\sum_{h=1}^{H-1} \tau_h^{-1} < W\zeta \leq \sum_{h=1}^H \tau_h^{-1} \quad (1)$$

$W = \sum_{h=1}^{N_{hops}} \tau_h^{-1}$ represents the sum of all possible migration event rates. The greater the rate of migration, the greater the probability of event H occurring in the duration migration period. N_A , N_B , and N_C represent the number of migration events for the bonds A, B, and C, respectively. The total number of migration events is recorded as m , and the total jump time of the walker is:

$$t = N_A \tau_A + N_B \tau_B + N_C \tau_C \quad (2)$$

When the walkers migrate enough steps, the mean square displacement $\langle r^2(t) \rangle$ is proportional to Dt , where D is the diffusion constant of the system. According to the Nernst–Einstein equation, D is in turn proportional to the total ionic conductivity σ :

$$\sigma = \frac{nq^2}{k_B T} D \quad (3)$$

where n is the carrier concentration, q is the charge, k_B is Boltzmann constant, and T is thermodynamic temperature. The carrier density n is determined by the concentration of the inorganic filler, p , which can be approximated as $n \sim pf$, where f is the filling fraction of all particles (polymers and inorganic fillers) in the composite conductor. In the simulation, 200 initial matrix models are randomized, and 10 walkers in each matrix model are randomly migrated. Finally, the ionic conductivity

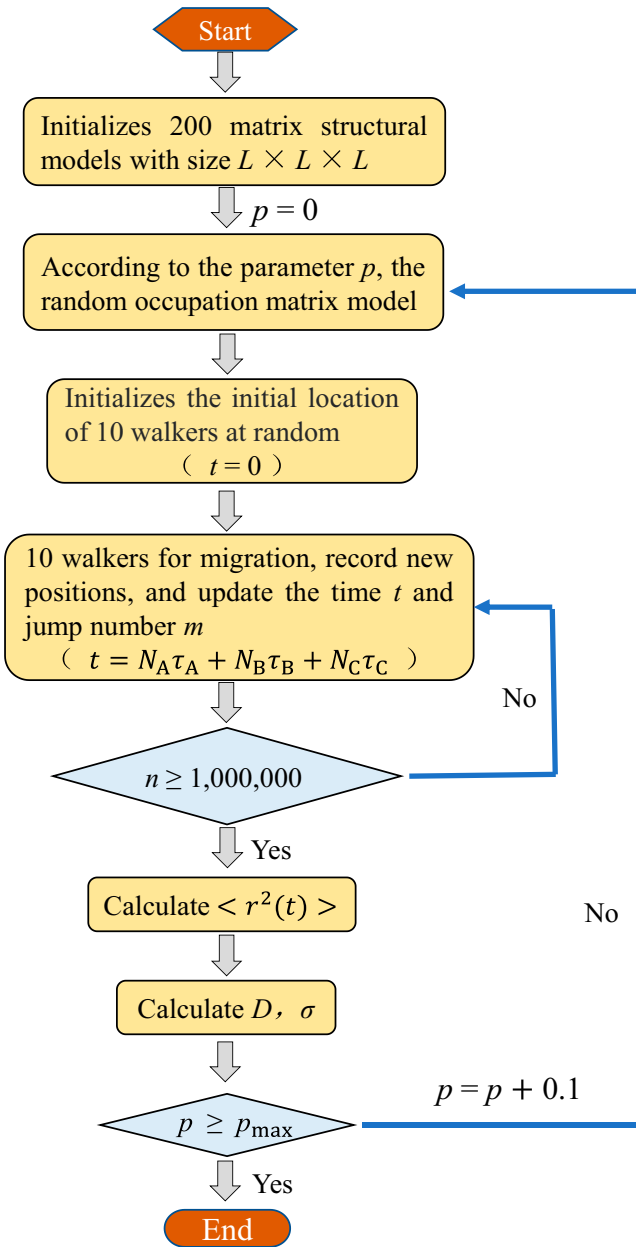


Fig. 4. The flowchart of ionic conductivity of IPCSEs calculated by random walk method based on RRM.

of all matrices is averaged. The calculation process is shown in Fig. 4.

Analytical calculation of ion conductivity through EMT

By changing the filling position of inorganic fillers in RRM (as shown in Fig. S1), the ionic conductivity of IPCSEs with different inorganic filler shapes can be evaluated. However, RRM cannot directly describe the size of inorganic fillers. Since the late 1970s, the EMT has been used to evaluate the conductivity of composite conductors and to study the effect of filler volume fraction and size on the ionic conductivity of IPCSEs [36,44–47]. Fig. 5 shows a 2-dimensional section of a composite conductor with NPs inorganic fillers. Here, IPCSEs are equivalent to 3-phase composites of low conductive polymer

matrix (σ_A), inorganic fillers (σ_B) and high conductive interfaces (σ_C).

The original EMT was developed for 2-phase (matrix phase and filler phase) composite materials. Table S3 summarizes several typical analytical equations for calculating conductivity for 2-phase composite conductor. However, the influence of the interface on the conductivity of the IPCSEs is crucial. In order to consider the interface region, Nan et al. improved the original EMT analytical equation [48,49]. They regard the filler and the interface as sub-composite fillers, and the conductivity is calculated from the original filler and the interface conductivity [50,51]. Taking the NPs fillers as an example (Fig. 2A), the effective ionic conductivity of the sub-composite filler (σ_1) is calculated according to the Maxwell-Wagner theory:

$$\frac{\sigma_1 - \sigma_B}{\sigma_1 + 2\sigma_B} = (1 - g_b) \frac{\sigma_C - \sigma_B}{\sigma_C + 2\sigma_B} \quad (4)$$

where σ_B and σ_C are the ionic conductivity of inorganic filler and interface phase, respectively; g_b is the volume fraction of inorganic filler in sub-composite fillers, which can be expressed as:

$$g_b = \frac{R^3}{(R + \lambda)^3} = \frac{1}{(1 + \gamma)^3} \quad (5)$$

where R is the radius of NPs, λ is the interface thickness, and $\gamma = \lambda/R$ is the dimensionless interface layer thickness parameter. The parameter g_a in Table S3, McLachlan Generalized Effective Medium Theory (GEMT), is replaced by $\frac{g_a}{g_b}$, which represents the volume percentage of the sub-composite fillers in the system. The revised GEMT is:

$$\left(\frac{g_a}{g_b}\right) \frac{\sigma_1^{1/t'} - \sigma_e^{1/t'}}{\sigma_1^{1/t'} + (1/g_{e1} - 1)\sigma_e^{1/t'}} + \left(1 - \frac{g_a}{g_b}\right) \frac{\sigma_1^{1/t'} - \sigma_e^{1/t'}}{\sigma_1^{1/t'} + (1/g_{e1} - 1)\sigma_e^{1/t'}} = 0 \quad (6)$$

where g_{e1} is the first percolation threshold (equivalent to p' in the Calculation of ionic conductivity based on random resistance model section) and t' is the first percolation slope. As described in the Calculation of ionic conductivity based on random resistance model section, due to the existence of 2 percolation thresholds, the ionic conductivity of the composite conductor will first increase to a maximum and then decrease. In the first region, the increase in conductivity is mainly attributed to the increase in the proportion of highly conductive interface phase, and the above formula is effective for this region. When $g_a = g_b$, the system is basically

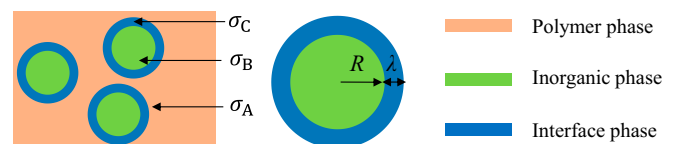


Fig. 5. Schematic diagram of the IPCSE microstructure (R and λ are the radius of nano-particles and the interface thickness, respectively).

represented by the interface phase and the inorganic filler phase. As the volume fraction of the inorganic filler increases, the volume fraction of the interface phase decreases, resulting in a decrease in conductivity. In this region, Eq. 6 needs to be changed to:

$$g_a \frac{\sigma_B^{1/t''} - \sigma_e^{1/t''}}{\sigma_B^{1/t''} + (1/g_{e2} - 1)\sigma_e^{1/t''}} + (1 - g_a) \frac{\sigma_C^{1/t''} - \sigma_e^{1/t''}}{\sigma_C^{1/t''} + (1/g_{e2} - 1)\sigma_e^{1/t''}} = 0 \quad (7)$$

where g_{e2} is the second percolation threshold (equivalent to p^* in the Calculation of ionic conductivity based on random resistance model section); t'' is the second percolation slope. In this work, the values of g_{e1} and g_{e2} are 0.28 and 0.15, respectively [45,51]. Generally, the greater difference between the conductivity of the polymer and the inorganic filler, the larger the value of t' and t'' . Here, we assume $t' = t'' = 1$; it can reduce the variables involved in the calculation.

Results and Discussion

In this section, the effect of the morphology of inorganic fillers on the ionic conductivity of IPCSEs is evaluated by the method in Methods from the 3 perspectives of the shape, arrangement, and size of inorganic fillers.

Effect of shapes of inorganic fillers on ionic conductivity of IPCSEs

Based on RRM, the composite conductor models of different shape fillers are built (NPs, NWs, NSs, and NNs, as shown in Fig. S1), and the ionic conductivity is calculated in each case by the random walk method. The ionic conductivity of the 3 phases in IPCSEs obtained from the corresponding references are listed in Table S2. The supporting information also elaborates on the setting of the parameters in the simulation.

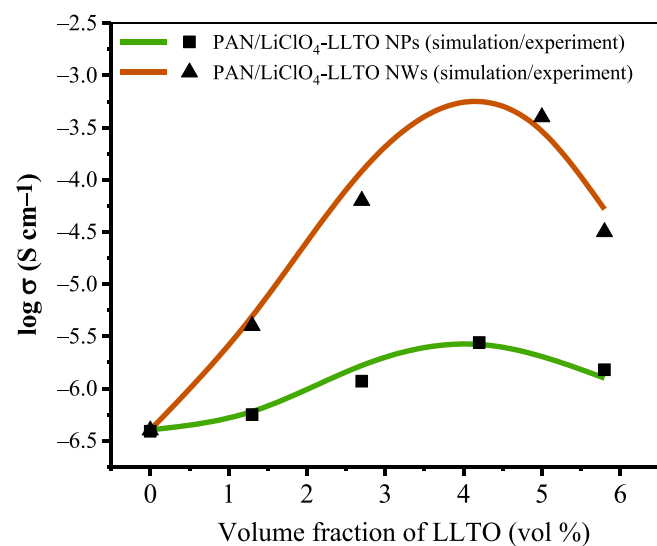


Fig. 6. The relationship between the ionic conductivity of PAN/LiClO₄-LLTO (NPs/NWs) and the volume fraction of LLTO (at room temperature). The real line is the simulated value, and the discrete points are the experimental value.

Figure 6 shows the experimental data and simulation results of ionic conductivity of PAN/LiClO₄+NPs/NWs-LLTO at room temperature. When the volume fraction of NPs-LLTO is 4 vol %, the ionic conductivity of PAN/LiClO₄+NPs-LLTO ($2.74 \times 10^{-6} \text{ S cm}^{-1}$) is only 6 to 7 times that of the polymer matrix ($4.1 \times 10^{-7} \text{ S cm}^{-1}$). However, when the filler is NWs-LLTO, the maximum ionic conductivity of PAN/LiClO₄+NWs-LLTO is $2.9 \times 10^{-4} \text{ S cm}^{-1}$, which is 3 orders of magnitude higher than that of the polymer matrix, and the corresponding optimal filler volume fraction (4.5 vol %) is higher than that of NPs-LLTO (4 vol %). The main reasons for this result is the low aspect ratio of NPs fillers, which makes it necessary for Li ions to pass through a large number of junctions with low conductivity formed by particle intersection. However, NWs fillers with high aspect ratio filled in polymer matrix can generate long and continuous Li ions' migration paths, so there exist fewer junctions, making the percolation conduction easier.

In addition, the trend of the ionic conductivity of IPCSEs in Fig. 6 shows that with the increase of the volume fraction of inorganic fillers, the ionic conductivity increases to a maximum value and then decreases, which is consistent with the percolation conduction phenomenon. The reason is that on the initial addition of inorganic fillers, high conductive interfaces begin to appear. As the filler continues to be added, these interfaces can be connected to form long-range conductive percolation paths, promoting ion conduction. However, the excessive volume fraction of fillers makes NPs fillers or NWs fillers easy to aggregate into clusters (as shown in Fig. 7), causing the migration path of high conductive ions in the IPCSEs truncated, so the ionic conductivity reaches a maximum and then begins to decrease.

Compared with NPs fillers, the aspect ratio of NSs fillers is also larger, and it is easier to form interfaces percolation paths in IPCSEs. Figure 8 shows the experimental data and simulation results of ionic conductivity of PEO/LiClO₄+NPs/NSs-LLZNO at room temperature. PEO/LiClO₄+5.1 vol %-NSs-LLZNO has superior ionic conductivity, with the maximum value of $3.71 \times 10^{-4} \text{ S cm}^{-1}$, which is 4 orders of magnitude higher than PEO/LiClO₄ ($\sim 2 \times 10^{-8} \text{ S cm}^{-1}$), and it is about 3 times higher than the highest ionic conductivity of PEO/LiClO₄+NPs-LLZNO ($1.25 \times 10^{-4} \text{ S cm}^{-1}$). When the volume fraction of NSs-LLZNO is 1.6 vol % to 5.1 vol %, the ionic conductivity increases, and then decreases significantly at 8.9 vol %. The superior properties of NSs fillers compared to NPs fillers is due to the

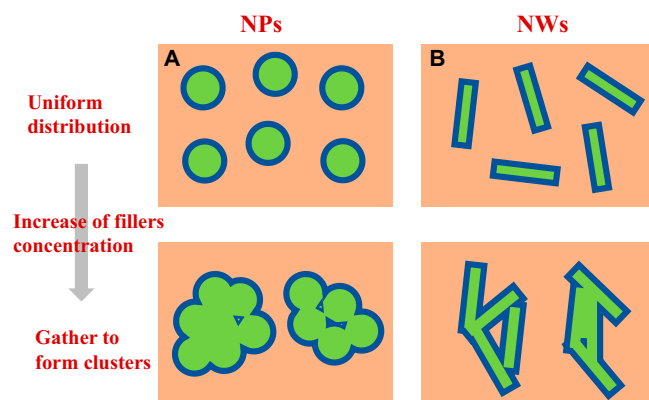


Fig. 7. With the increase of inorganic fillers, (A) NPs and (B) NWs change from uniform distribution into clusters.

high aspect ratio of nanosheets, i.e., fewer filler–filler junctions, which promotes ion conduction.

We also use the same method to calculate the ionic conductivity of PEO/LiTFSI filled with NPs-LLTO and NNs-LLTO, and the results are shown in Fig. 9. When the volume fraction of NPs-LLTO is 4 vol %, the ionic conductivity of IPCSEs

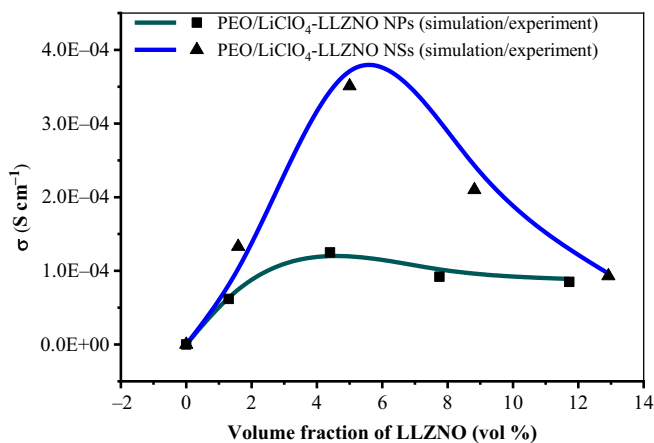


Fig. 8. The relationship between the ionic conductivity of PEO/LiClO₄-LLZNO (NPs/NSs) and the volume fraction of LLZNO (at room temperature). The real line is the simulated value, and the discrete points are the experimental value.

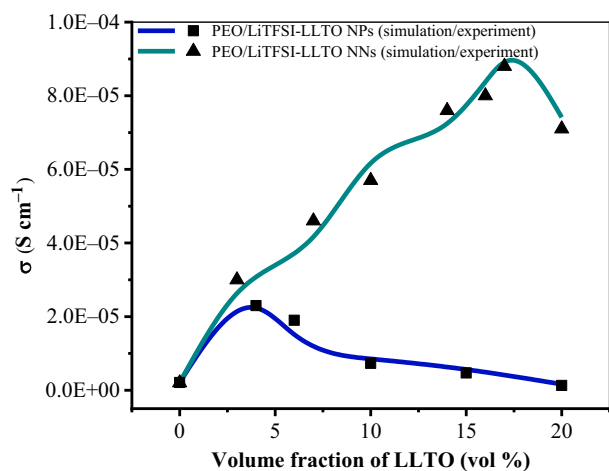


Fig. 9. The relationship between the ionic conductivity of PEO/LiTFSI-LLTO (NPs/NNs) and the volume fraction of LLTO (at room temperature). The real line is the simulated value, and the discrete points are the experimental value.

reaches the maximum value and then begins to decrease, and NPs-LLTO begins to form clusters at a lower volume fraction. Obviously, NNs fillers can be filled at a large volume fraction compared to NPs, NWs, or NSs. For the NNs-LLTO, the optimal filling volume fraction can reach 17 vol %, and the ionic conductivity of PEO/LiTFSI+NNs-LLTO is 4 to 5 times that of PEO/LiTFSI+NPs-LLTO (PEO/LiTFSI+NPs-LLTO: $\sim 1.9 \times 10^{-5} \text{ S cm}^{-1}$, PEO/LiTFSI+NNs-LLTO: $\sim 8.9 \times 10^{-5} \text{ S cm}^{-1}$). As expected, the results presented above show that among NPs, NWs, NSs, and NNs fillers, the latter provide the most beneficial effects, due to their inherent percolation structure. The calculation results are also in good quantitative agreement with the experimental values [12,52,53].

According to our calculations, the shape of the inorganic filler directly determines the length and dimensionality of the high-conductivity interface path, and the inorganic fillers of various shapes have different enhancement effects on the ionic conductivity of IPCSEs at different filling levels.

Effect of the arrangement of inorganic fillers on the ionic conductivity of IPCSEs

From the calculation examples of the Effect of shapes of inorganic fillers on ionic conductivity of IPCSEs section, it can be observed that the random filling of NPs, NWs, and even NSs fillers in the polymer matrix will easily aggregate into clusters at a certain volume fraction. Substantial inorganic filler agglomeration significantly reduces the volume percentage of the interface phase in the IPCSEs, disrupting the percolation paths of the interface phase and lowering the ionic conductivity. In addition, random spatial distribution of the inorganic filler causes the interfacial paths to be randomly and disorderly arranged in the IPCSEs as well, hindering formation of percolation paths. Controlled arrangement of inorganic fillers can be used to maximize percolation. Figure S2 shows the schematic diagram of the ordered arrangement of inorganic fillers in solid electrolyte. When the inorganic fillers are distributed along the direction perpendicular to the solid electrolyte interface (SEI), the ion migration path can directly connect the 2 electrodes, allowing Li ions to migrate between the 2 electrodes in the shortest distance and in the fastest way.

In this section, we calculate the ionic conductivity of IPCSEs when the inorganic fillers considered in the Effect of shapes of inorganic fillers on ionic conductivity of IPCSEs section are arranged in an ordered way. Table compares the highest ionic conductivity of IPCSEs at room temperature and the corresponding optimal volume fraction of inorganic fillers under these 2 arrangements (ordered or disordered arrangement). It can be observed that IPCSEs with ordered inorganic fillers have

Table. Comparison of the σ_{\max} and v_{opt} of IPCSEs with 2 different arrangements of inorganic fillers (at room temperature). v_{opt} is the optimal filling volume fraction of inorganic fillers; σ_{\max} is the highest ionic conductivity of IPCSEs.

IPCSEs	PAN/LiClO ₄ -LLTO (NWs)		PEO/LiClO ₄ -LLZNO (NSs)		PEO/LiTFSI-LLTO (NNs)	
	Disordered	Ordered	Disordered	Ordered	Disordered	Ordered
v_{opt} (vol %)	5	15	5	16	17	20
σ_{\max} (S cm ⁻¹)	2.9×10^{-4}	4.7×10^{-4}	3.7×10^{-4}	7.8×10^{-4}	8.9×10^{-5}	4.5×10^{-4}

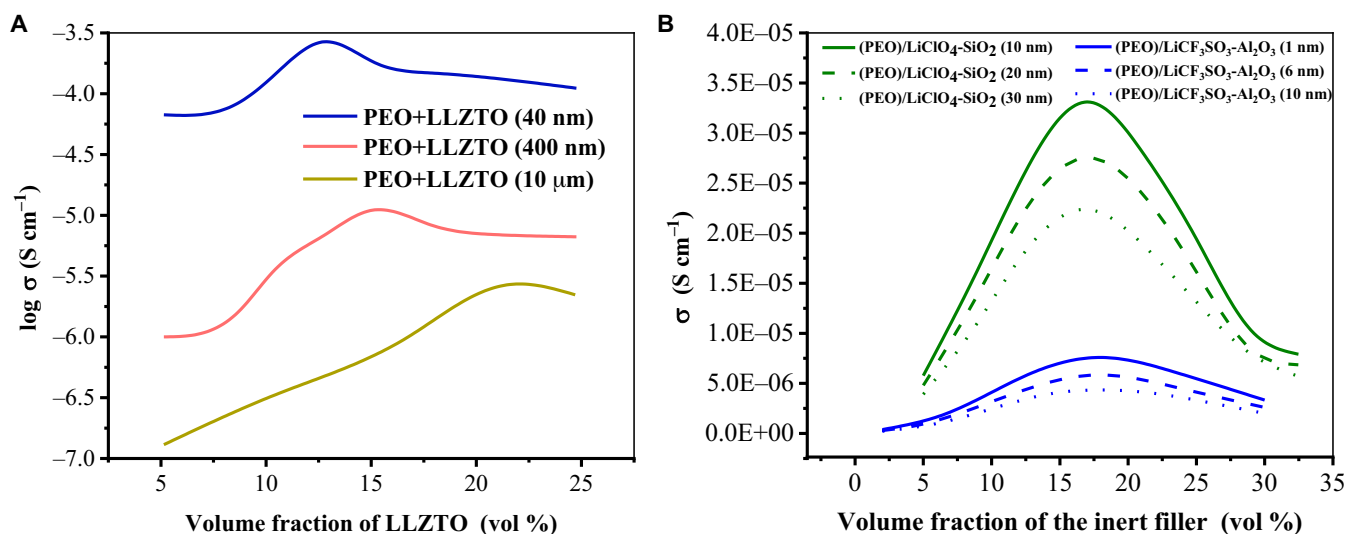


Fig. 10. (A) Relationship between the ionic conductivity of PEO-LLZTO and the grain size of NPs-LLZTO. (B) Relationship between the ionic conductivity of IPCSEs and the grain size of inert filler (PEO/LiClO₄-SiO₂, PEO/LiCF₃SO₃-Al₂O₃) (at room temperature).

higher ionic conductivity, which is 2 to 6 times higher than the corresponding disordered arrangement. We note that the calculation results of this section have not been verified by experiments, but they are in line with our expectations.

Effect of size of inorganic particles on ionic conductivity of IPCSEs

In addition to topology, arising from different shape of the fillers, discussed in the Effect of shapes of inorganic fillers on ionic conductivity of IPCSEs section, it is important to consider the effect of their geometry. In this section, we calculate the ionic conductivity of IPCSEs with different NPs grain sizes using the method in the Analytical calculation of ion conductivity through EMT section. Figure 10A shows the ionic conductivity of PEO filled with NPs-LLZTO with different grain sizes (40 nm, 400 nm, and 10 μm). When the grain size of LLZTO is 40 nm, 400 nm, and 10 μm , the highest ionic conductivity of IPCSEs is $2.6 \times 10^{-4} \text{ S cm}^{-1}$, $1.1 \times 10^{-5} \text{ S cm}^{-1}$, and $2.7 \times 10^{-6} \text{ S cm}^{-1}$, respectively. The simulation results are in good agreement with the experimental results [23]. In addition, the smaller the size of NPs-LLZTO, the more easily can IPCSEs obtain the best conductivity at low inorganic filler volume ratio. As shown in Fig. 10A, as the size of NPs-LLZTO increases, the corresponding optimal volume fractions are 12 vol %, 15 vol %, and 21 vol %, respectively. The main reason for this phenomenon is that the smaller the size of the NPs, the larger the specific surface area around the active sites, which can effectively reduce the crystallization of the polymer matrix and enhance the dissociation of the lithium salt, thus providing more conduction paths for Li ions.

In addition to the active filler, the inert fillers, e.g., SiO₂ and Al₂O₃, also have an effect on the ionic conductivity of the IPCSEs. We predicted the relationship between the ionic conductivity of PEO/LiClO₄-SiO₂, PEO/LiCF₃SO₃-Al₂O₃, and the inert filler grain size (as shown in Fig. 10B).

Ultimately, it can be concluded that for the certain inert inorganic filler and polymer matrix, the overall ionic conductivity of the corresponding IPCSEs increases with decreasing particle size of the inert inorganic filler.

Conclusion

To model the effect of size, shape, and arrangement of inorganic fillers in a polymer matrix on percolation conduction in IPCSEs, software was developed using python. The software combines RRM and EMT. The test results show that the ionic conductivity of IPCSEs with NWs, NSs, and NNs of inorganic fillers is higher than that with NPs at the same loading level. In addition, compared with the disordered arrangement of inorganic fillers, ordered arrangement provides the more effective and faster percolation paths and promotes ion conduction. The results of EMT analytical calculations also demonstrate the effect of the grain size of inorganic NPs on the ionic conductivity of IPCSEs; that is, small size particles improve the ionic conductivity of IPCSEs. It is worth mentioning that the parameters required for calculations are related to ionic conductivity of the polymer phase, inorganic phase, and interface phase, which are obtained by experimental measurements. Although limited experimental reference data are available at the moment, the results of the calculations are in good quantitative agreement. In addition to evaluating the ionic conductivity of IPCSEs, the method is also applicable to other types of 2-phase composite conductors, such as inorganic-inorganic composites, and the software is expected to become a reliable pre-screening tool for composite electrolytes, providing valuable guidance for experimental research.

Acknowledgments

We are grateful to the developers of the pymatgen python library [54]. **Funding:** This work was supported by the National Key Research and Development Program of China (No. 2021YFB3802104), the National Natural Science Foundation of China (Nos. U2030206 and 11874254), and the Shanghai Municipal Science and Technology Commission (No. 19DZ2252600). **Author contributions:** Y.D. wrote the initial draft of the manuscript. Y.D. and B.H. jointly developed the program. M.A., Y.L., and D.W. helped to revise the manuscript. S.S. was responsible for the conceptualization, writing, and management. All authors

read and approved the final manuscript. **Competing interests:** The authors declare that they have no competing interests.

Data Availability

The authors declare that the main data supporting the finding of this study are available within the article or supporting information. Extra data are available from the corresponding author upon reasonable request. All source codes of the software are implemented in Python and uploaded to the code repository: <https://gitlab.com/bmaterials/erpicp>.

Supplementary Materials

Fig. S1 and S2
Table S1 to S3

References

- Zou Z, Li Y, Lu Z, Wang D, Cui Y, Guo B, Li Y, Liang X, Feng J, Li H, et al. Mobile ions in composite solids. *Chem Rev.* 2020;120(9):4169–4221.
- Lopez J, Mackanic DG, Cui Y, Bao Z. Designing polymers for advanced battery chemistries. *Nat Rev Mater.* 2019;4:312–330.
- Mindemark J, Lacey MJ, Bowden T, Brandell D. Beyond PEO—alternative host materials for Li⁺-conducting solid polymer electrolytes. *Prog Polym Sci.* 2018;81:114–143.
- Zhao Q, Stalin S, Zhao CZ, Archer LA. Designing solid-state electrolytes for safe, energy-dense batteries. *Nat Rev Mater.* 2020;5:229–252.
- Famprikis T, Canepa P, Dawson JA, Islam MS, Masquelier C. Fundamentals of inorganic solid-state electrolytes for batteries. *Nat Mater.* 2019;18:1278–1291.
- Ren Y, Chen K, Chen R, Liu T, Zhang Y, Nan CW. Oxide electrolytes for lithium batteries. *J Am Ceram Soc.* 2015;98:3603–3623.
- Wang C, Fu K, Kammampata SP, McOwen DW, Samson AJ, Zhang L, Hitz GT, Nolan AM, Wachsmann ED, Mo Y, et al. Garnet-type solid-state electrolytes: Materials, interfaces, and batteries. *Chem Rev.* 2020;120(10):4257–4300.
- Li X, Liang J, Yang X, Adair KR, Wang C, Zhao F, Sun X. Progress and perspectives on halide lithium conductors for all-solid-state lithium batteries. *Energy Environ Sci.* 2020;13(5):1429–1461.
- Chen R, Li Q, Yu X, Chen L, Li H. Approaching practically accessible solid-state batteries: Stability issues related to solid electrolytes and interfaces. *Chem Rev.* 2019;120(14):6820–6877.
- Tan DH, Banerjee A, Chen Z, Meng YS. From nanoscale interface characterization to sustainable energy storage using all-solid-state batteries. *Nat Nanotechnol.* 2020;15(3):170–180.
- Fenton D, Parker JM, Wright PV. Complexes of alkali metal ions with poly(ethylene oxide). *Polymer.* 1973;14(73):589.
- Liu W, Liu N, Sun J, Hsu P-C, Li Y, Lee H-W, Cui Y. Ionic conductivity enhancement of polymer electrolytes with ceramic nanowire fillers. *Nano Lett.* 2015;15(4):2740–2745.
- Zhang X, Liu T, Zhang S, Huang X, Xu B, Lin Y, Xu B, Li L, Nan C-W, Shen Y. Synergistic coupling between Li_{6.75}La₃Zr_{1.75}Ta_{0.25}O₁₂ and poly(vinylidene fluoride) induces high ionic conductivity, mechanical strength, and thermal stability of solid composite electrolytes. *J Am Ceram Soc.* 2017;139(39):13779–13785.
- Jian Z, Hu YS, Ji X, Chen W. Nasicon-structured materials for energy storage. *Adv Mater.* 2017;29(20):Article 1601925.
- Stramare S, Thangadurai V, Weppner W. Lithium lanthanum titanates: A review. *Chem Mater.* 2003;15:3974–3990.
- Thangadurai V, Narayanan S, Pinzaru D. Garnet-type solid-state fast Li ion conductors for Li batteries: Critical review. *Chem Soc Rev.* 2014;43(13):4714–4727.
- Zhao N, Khokhar W, Bi Z, Shi C, Guo X, Fan L-Z, Nan C-W. Solid garnet batteries. *Joule.* 2019;3(5):1190–1199.
- Fan LZ, He H, Nan CW. Tailoring inorganic–polymer composites for the mass production of solid-state batteries. *Nat Rev Mater.* 2021;6:1003–1019.
- Zheng J, Tang M, Hu YY. Lithium ion pathway within Li₇La₃Zr₂O₁₂-polyethylene oxide composite electrolytes. *Angew Chem Int Ed.* 2016;55(40):12538–12542.
- Zheng J, Hu Y-Y. New insights into the compositional dependence of Li-ion transport in polymer–ceramic composite electrolytes. *ACS Appl Mater Interfaces.* 2018;10(4):4113–4120.
- Yang T, Zheng J, Cheng Q, Hu Y-Y, Chan CK. Composite polymer electrolytes with Li₇La₃Zr₂O₁₂ garnet-type nanowires as ceramic fillers: Mechanism of conductivity enhancement and role of doping and morphology. *ACS Appl Mater Interfaces.* 2017;9(26):21773–21780.
- Zheng J, Wang P, Liu H, Hu Y-Y. Interface-enabled ion conduction in Li₁₀GeP₂S₁₂-poly(ethylene oxide) hybrid electrolytes. *ACS Appl Energy Mater.* 2019;2(2):1452–1459.
- Zhang J, Zhao N, Zhang M, Li Y, Chu PK, Guo X, Di Z, Wang X, Li H. Flexible and ion-conducting membrane electrolytes for solid-state lithium batteries: Dispersion of garnet nanoparticles in insulating polyethylene oxide. *Nano Energy.* 2016;28:447–454.
- Lin D, Liu W, Liu Y, Lee HR, Hsu P-C, Liu K, Cui Y. High ionic conductivity of composite solid polymer electrolyte via in situ synthesis of monodispersed SiO₂ nanospheres in poly(ethylene oxide). *Nano Lett.* 2016;16(1):459–465.
- Zhu P, Yan C, Dirican M, Zhu J, Zang J, Selvan RK, Chung CC, Jia H, Li Y, Kiyak Y, et al. Li_{0.33}La_{0.57}TiO₃ ceramic nanofiber-enhanced polyethylene oxide-based composite polymer electrolytes for all-solid-state lithium batteries. *J Mater Chem A.* 2018;6(10):4279–4285.
- Wan Z, Lei D, Yang W, Liu C, Shi K, Hao X, Shen L, Lv W, Li B, Yang QH, et al. Low resistance-integrated all-solid-state battery achieved by Li₇La₃Zr₂O₁₂ nanowire upgrading polyethylene oxide (PEO) composite electrolyte and PEO cathode binder. *Adv Funct Mater.* 2019;29(1):Article 1805301.
- Wu N, Chien PH, Li Y, Dolocan A, Xu H, Xu B, Grundish NS, Jin H, Hu YY, Goodenough JB. Fast Li⁺ conduction mechanism and interfacial chemistry of a NASICON/polymer composite electrolyte. *J Am Ceram Soc.* 2020;142(5):2497–2505.
- Xu H, Chien PH, Shi J, Li Y, Wu N, Liu Y, Hu Y-Y, Goodenough J-B. High-performance all-solid-state batteries enabled by salt bonding to perovskite in poly(ethylene oxide). *PNAS.* 2019;116(38):18815–18821.
- Wu N, Chien P-H, Qian Y, Li Y, Xu H, Grundish NS, Xu B, Jin H, Hu Y-Y, Yu G, et al. Enhanced surface interactions enable fast Li⁺ conduction in oxide/polymer composite electrolyte. *Angew Chem Int Ed.* 2020;59(10):4131–4137.
- Gong Y, Fu K, Xu S, Dai J, Hamann TR, Zhang L, Hitz GT, Fu Z, Ma Z, McOwen DW, et al. Lithium-ion conductive ceramic textile: A new architecture for flexible solid-state lithium metal batteries. *Mater Today.* 2018;21(6):594–601.
- Li Z, Sha W-X, Guo X. Three-dimensional garnet framework-reinforced solid composite electrolytes with high lithium-ion

- conductivity and excellent stability. *ACS Appl Mater Interfaces*. 2019;11(30):26920–26927.
32. Li Y, Zhao Y, Cui Y, Zou Z, Wang D, Shi S. Screening polyethylene oxide-based composite polymer electrolytes via combining effective medium theory and Halpin-Tsai model. *Comput Mater Sci*. 2018;144:338–344.
 33. Bunde A, Dieterich W, Roman E. Dispersed ionic conductors and percolation theory. *Phys Rev Lett*. 1985;55(1):5–8.
 34. Roman H, Bunde A, Dieterich W. Conductivity of dispersed ionic conductors: A percolation model with two critical points. *Phys Rev B Condens Matter*. 1986;34(5):3439–3445.
 35. Li Z, Huang HM, Zhu JK, Wu JF, Yang H, Wei L, Guo X. Ionic conduction in composite polymer electrolytes: Case of PEO: Ga-LLZO composites. *ACS Appl Mater Interfaces*. 2018;11(1):784–791.
 36. Nan C-W, Smith DM. A.c. electrical properties of composite solid electrolytes. *Mater Sci Eng B*. 1991;10(2):99–106.
 37. Nan CW. Physics of inhomogeneous inorganic materials. *Prog Mater Sci*. 1993;37(1):1–116.
 38. Nan C-W. Conduction theory of ionic conductor containing dispersed second phase. *Acta Phys Sin*. 1987;36(2):191–198.
 39. De Gennes PG. La Percolation: Un concept unificateur. *La recherche*. 1976;7:919–927.
 40. De Gennes PG. Percolation: Quelques systemes nouveaux. *J Phys Colloques*. 1980;41:C3-17–C3-26.
 41. Havlin S, Ben-Avraham D. Diffusion in disordered media. *Adv Phys*. 1987;36(1-2):695–798.
 42. Blanc R. Introduction to percolation theory. In: *Contribution of clusters physics to materials science and technology: From isolated clusters to aggregated materials*. Springer Dordrecht; 1986.
 43. Majid I, Ben-Avraham D, Havlin S, Stanley HE. Exact-enumeration approach to random walks on percolation clusters in two dimensions. *Phys. Rev*. 1984;30:Article 1626.
 44. Stoneham A, Wade E, Kilner J. A model for the fast ionic diffusion in alumina-doped LiI. *Mater Res Bull*. 1979;14(5):661–666.
 45. Han DG, Choi GM. Computer simulation of the electrical conductivity of composites: The effect of geometrical arrangement. *Solid State Ionics*. 1998;106(1-2):71–87.
 46. Roman H. A continuum percolation model for dispersed ionic conductors. *J Phys: Condens Matt*. 1990;2:Article 3909.
 47. Kalnaus S, Sabau AS, Tenhaeff WE, Dudney NJ, Daniel C. Design of composite polymer electrolytes for Li ion batteries based on mechanical stability criteria. *J Power Sources*. 2012;201:280–287.
 48. Przulski J, Siekierski M, Wiczonek W. Effective medium theory in studies of conductivity of composite polymeric electrolytes. *Electrochim Acta*. 1995;40(13-14):2101–2108.
 49. Wiczonek W, Zalewska A, Siekierski M, Przulski J. Modelling the ac conductivity behaviour of composite polymeric electrolytes by the effective medium theory. *Solid State Ionics*. 1996;86:357–362.
 50. Nan CW, Fan L, Lin Y, Cai Q. Enhanced ionic conductivity of polymer electrolytes containing nanocomposite SiO₂ particles. *Phys Rev Lett*. 2003;91:Article 266104.
 51. Wiczonek W, Siekierski M. A description of the temperature dependence of the conductivity for composite polymeric electrolytes by effective medium theory. *J Appl Phys*. 1994;76(4):2220–2226.
 52. Song S, Wu Y, Tang W, Deng F, Yao J, Liu Z, Hu R, Alamus, Wen Z, Lu L, et al. Composite solid polymer electrolyte with garnet nanosheets in poly(ethylene oxide). *ACS Sustainable Chem Eng*. 2019;7(7):7163–7170.
 53. Bae J, Li YT, Zhang J, Zhou XY, Zhao F, Shi Y, Goodenough JB, Yu G. A 3D nanostructured hydrogel-framework-derived high-performance composite polymer lithium-ion electrolyte. *Angew Chem Int Ed*. 2018;57(8):2096–2100.
 54. Ong SP, Richards WD, Jain A, Hautier G, Kocher M, Cholia S, Gunter D, Chevrier VL, Persson KA, Ceder G. Python materials genomics (pymatgen): A robust, open-source python library for materials analysis. *Comput Mater Sci*. 2013;68:314–319.